Chain Conformation and Hydration of PEO Grafted to Gold Nanoparticles: Curvature and Chain Length Effect

Udaya Dahal and Elena E. Dormidontova*

Polymer Program, Institute of Materials Science and Physics Department, University of Connecticut, Storrs, Connecticut 06269, United States

Table of contents graphic:

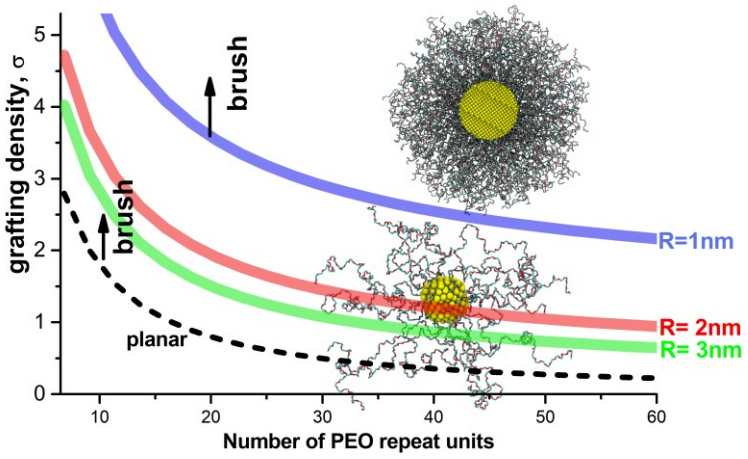

Abstract.

Development of functional polymer-grafted nanoparticles for various nanotechnological applications, including nanomedicine, requires understanding of the interplay of design parameters governed by the underlying polymer physics principles. Using atomistic molecular dynamics simulation we investigate hydration and structural properties of spherical gold nanoparticles (1nm and 3nm radius) with grafted polyethylene oxide (PEO) of different lengths at two grafting densities. We demonstrate that the criterion for planar surfaces is insufficient to achieve the brush regime for nanoparticles of high curvature, as the chain conformation and hydration remain very similar to aqueous solution thereby exposing the nanoparticle surface, which may compromise the stealth properties of PEO-grafted nanoparticles. A new criterion for achieving the brush regime is proposed accounting for nanoparticle curvature. At high grafting density ($4.2nm^{-2}$) we find that the PEO brush is rather dense and partially dehydrated in the vicinity of the gold nanoparticle surface in agreement with experimental observations. In contrast to experimental assumptions and some analytical predictions, we find that polymer density decreases with radial distance as $r^{-4/3}$ throughout the brush including the dense region, where PEO chains are stretched and oriented independent of PEO length. Chain stretching and orientation lead to a $N^{4/5}$ scaling dependence for the brush height, which is stronger than classical theoretical predictions, but agrees with reported experimental data. PEO tail flexibility, which is relevant for inhibition of protein adsorption, is found to increase substantially with chain length and distance from the nanoparticle core.

Introduction

Nanoparticles grafted with bio(compatible)polymers are actively studied for biomedical applications.[1–6] In particular, gold nanoparticles have been intensely investigated due to their low toxicity, ability to produce local heating and plasmonic properties making them desirable for photodynamic therapy, cell imaging and biosensing.[4,7] To ensure nanoparticle dispersion, long-time circulation, protection from non-specific protein adsorption and impose functionality, e.g. attachment of drugs or targeting groups, nanoparticles are grafted by biopolymers or biocompatible polymers, most commonly poly(ethylene) oxide (PEO) due to its capability to inhibit protein adsorption.[1,4,5,7,8] For a given nanoparticle size there is a choice of grafting densities and polymer molecular weights to use.[1,3,6,7,9–11] The choice is often made based on available material and common wisdom of achieving a brush structure for planar surfaces, i.e. at least one chain per nm^2.[2,12] While there are some systematic studies exploring a range of nanoparticle sizes and PEO grafting densities,[4,5,8,11,13,14] the general understanding of the effect of PEO chain length on the structure and properties of grafted spherical layers of PEO remains unclear, especially as concerns gold nanoparticles of small sizes,[15] i.e. high curvature, and the PEO conformation and hydration properties within the layer. In this paper we investigate by means of atomistic molecular dynamics simulations the effect of PEO length on chain conformation and hydration of PEO in grafted spherical layers of moderate and high grafting density for small gold nanoparticles and make predictions that can be useful for further experimental development of PEO-grafted nanoparticles.

The effect of chain length on the properties and performance PEO-grafted spherical nanoparticles has been studied experimentally[7,10,11,16] with the results and conclusions varying from study to study. Some concluded that there is a preference for a longer PEO length to achieve improved

circulation and prevention of protein adsorption, but the results depend also on nanoparticle size, i.e. curvature and grafting density and specific application (e.g. penetration of brain-blood barrier or cell internalization efficiency).[1–3,5–7] Maintaining a high level of hydration and flexibility of PEO chains in a brush are considered among the important factors influencing protein adsorption.[2,5,8,17–19] The interconnection of chain length, grafting density and nanoparticle size with polymer chain mobility and hydration within a grafted polymer layer is not an easy question to address, as these properties are not readily measured experimentally. Computer simulations can provide necessary insights to these characteristics but require an atomistic level of resolution and as such are limited to relatively small nanoparticles and PEO chain lengths. Recently the effect of grafting density on chain conformation and hydration of PEO grafted to gold or TiO_2 nanoparticles has been studied by computer simulations[12,14,20,21] for a given chain length. From a theoretical perspective a longer polymer chain length implies that the transition from the mushroom to brush regime for a flat surface occurs at a lower grafting density according to the criterion $\sigma^* \sim 1/R_{go}^2$, where R_{go} is the radius of gyration of a polymer chain in solution.[22] In the mushroom regime PEO chains should be well-hydrated and maintain their natural flexibility, but whether they provide sufficient protection of the surface from e.g. protein adsorption, remains in question, especially for strongly curved surfaces such as small spherical nanoparticles, where the area available per chain significantly increases away from the surface.[2,8] A range of gold nanoparticles of different sizes and shapes are achievable experimentally ranging from gold nanoclusters containing only a few Au atoms to a few nanometer gold nanoparticles.[15,23] In the particular case of gold nanoparticles there is also some propensity for PEO adsorption on the gold surface to compensate for water layering (due to loss of hydrogen bonding) as was reported experimentally and in computer simulation studies, including our previous work.[20,21,24] Perhaps a more interesting question is the

structure of a grafted PEO layer just above the overlap limit for the nanoparticle surface, i.e. for $\sigma \geq \sigma^* \sim 1/R_{go}^2$. Are the PEO chains stretched as in a brush, what is the extent of hydration throughout the grafted layer and how are these properties affected by chain length and nanoparticle size? We are not aware of any experimental or computer simulation studies on this subject which will be investigated and discussed in this paper.

In the opposite limit of high grafting density well into the brush regime PEO chains are expected to be crowded, so surface protection should be easily achieved. On the other hand, a high polymer density inside the layer may compromise hydration and chain mobility, which would be disadvantageous for prevention of protein adsorption.[25,26] Thus, several experimental studies[9,27,28] using SAXS and SANS measurements suggested that nanoparticles densely grafted by polymers exhibit a region of constant high density in the vicinity of nanoparticle surface. Inside a dense brush polymer hydration and mobility can be limited, but detailed analysis of these properties is hard to achieve experimentally. In this paper using atomistic molecular dynamics simulations we investigate hydration and tail flexibility of PEO chains in dense spherical brush for PEO chains of different length. The obtained density profiles and brush height will be compared with theoretical predictions and the results of experimental and previous computer simulation studies. In particular, the existence of a concentrated region near the nanoparticle surface will be examined. The obtained results can provide molecular level details of the hydration and chain conformation of spherical PEO polymer brushes and can bridge the gap between theory and experiments. Besides contributing to fundamental understanding of properties of spherical brushes, our results can also guide experimental development and improvement of existing nanomaterials for biomedical applications where polymer conformation and hydration can be important.

Simulation Details

We performed all-atom molecular dynamics simulations of 1 nm and 3nm in radius spherical gold nanoparticles grafted by methyl-terminated PEO chains of different molecular weights: N=12, N=20, N=36 and N=45 repeat units. We considered two cases of moderate grafting density σ=1.5 nm^{-2} and high grafting density σ=4.18 chains per nm^2, which is close to the maximum experimentally achieved grafting density.[1] To obtain an equilibrium structure of a dense spherical PEO brush, we started with coarse-grained molecular dynamics simulations using the Martini force field,[29,30] similar to what was done in our previous work discussing the grafting density effect.[20] The gold nanoparticle was modelled as a spherical particle of coarse-grained beads using the same force field as in our previous simulations.[20] To model a spherical structure in coarse-grained simulations, we generated a spherical shell of atoms anchored to a center atom by a bond equal to the radius of the sphere. PEO chains were homogeneously grafted to gold beads on the nanoparticle surface. The NPT coarse-grained simulations were run using the GPU version of GROMACS-4.6.5 for at least 500 ns to equilibrate the PEO-grafted gold nanoparticles (for details see supporting information). The equilibrated structure of PEO-grafted gold nanoparticles obtained in coarse-grained simulations was back-mapped[31] to an atomistic structure (as discussed in supporting information). For atomistic simulations the gold nanoparticle was generated using FCC crystalline gold cut into a spherical shape of 1 or 3nm radius. For gold we used the force field reported in the literature[32] as was done in our previous papers on planar and spherical PEO brushes.[20,21] PEO chains were roughly homogeneously attached to the surface of the gold nanoparticle via sulfur bonds. The force field parameters for PEO and sulfur were the same as in our previous papers.[20,21,33–35] The SPCE model for water was used in all simulations. Depending on the PEO chain lengths, the periodic box size varied from (17nm x 17nm x 17 nm) for shorter

chains to (30nm x 30nm x 30nm) for the longer ones. All simulations were carried out using the GPU version of GROMACS-4.6.5. We used an NPT ensemble to simulate the system using a V-rescale thermostat at T=310k and Berendsen barostat at pressure 1 atm to be consistent with our previous computer simulations. The coupling time constants for temperature was 1ps and for pressure 2ps. Electrostatic calculation was done using PME method with Fourier spacing 0.12nm. The integration time step for the simulation was 2fs. Each system was equilibrated for at least 25 ns to 60 ns.

The volume fraction radial distributions for PEO and water were calculated using spherical layers of $0.3\,nm$ width in the radial direction starting from the gold nanoparticle center of mass. For volume fraction calculations we used $0.02\,nm^3$ for the volume of the CH_2 group and oxygen of PEO and $0.03\,nm^3$ for the water volume, similar to our previous papers. [20,21] The hydrogen bond calculation was performed using the geometrical criteria for the distance between oxygens of PEO and water $r_{oo} \leq 3.5\,nm$ and angle between the vectors of hydrogen (H) to oxygen of water (satisfying the distance criterion) and oxygen of water (D) to oxygen of PEO (A) $\measuredangle HDA \leq 30^{\circ}$.

RESULTS AND DISCUSSION:

Moderate grafting density. As discussed in our previous publication and reported experimentally[20,21,24] at low to moderate grafting densities PEO chains exhibit some degree of adsorption to a gold surface (to substitute for water layering), which could also depend on the local morphology of Au atoms on the gold nanoparticle surface. Comparing 1nm gold nanoparticles grafted with PEO of different chain lengths, all at a grafting density of $1.5nm^{-2}$, as shown in Figure 1, one can notice that some segments of PEO chains indeed reside in the immediate vicinity of the

gold surface. This is especially noticeable for shorter chain lengths. Overall the structure of the spherical polymer layer looks rather diffuse and does not show brush-like features (Figure 1), which could be expected as $\sigma^* \sim 1/R_{go}^2$ is less than $1.5nm^{-2}$ for PEO with 15 or more repeat units (Table S2 of supporting information). Indeed, the polymer volume fraction profile shows that while near the surface the volume fraction of polymer reaches 0.5, it quickly decreases in an exponential-like manner away from the surface. The density profiles for PEO of different chain lengths coincide within about 1nm of the surface. Similar behavior is observed for 3mn gold nanoparticles grafted with PEO chains of 12 and 20 repeat units at the same grafting density of $1.5nm^{-2}$ (inset of Figure 1). The strong decay of the polymer volume fraction away from the surface implies free water access to the nanoparticle surface, as will be discussed below, indicating that this grafting density may not provide sufficient protection of the core.[2,3,5,7]

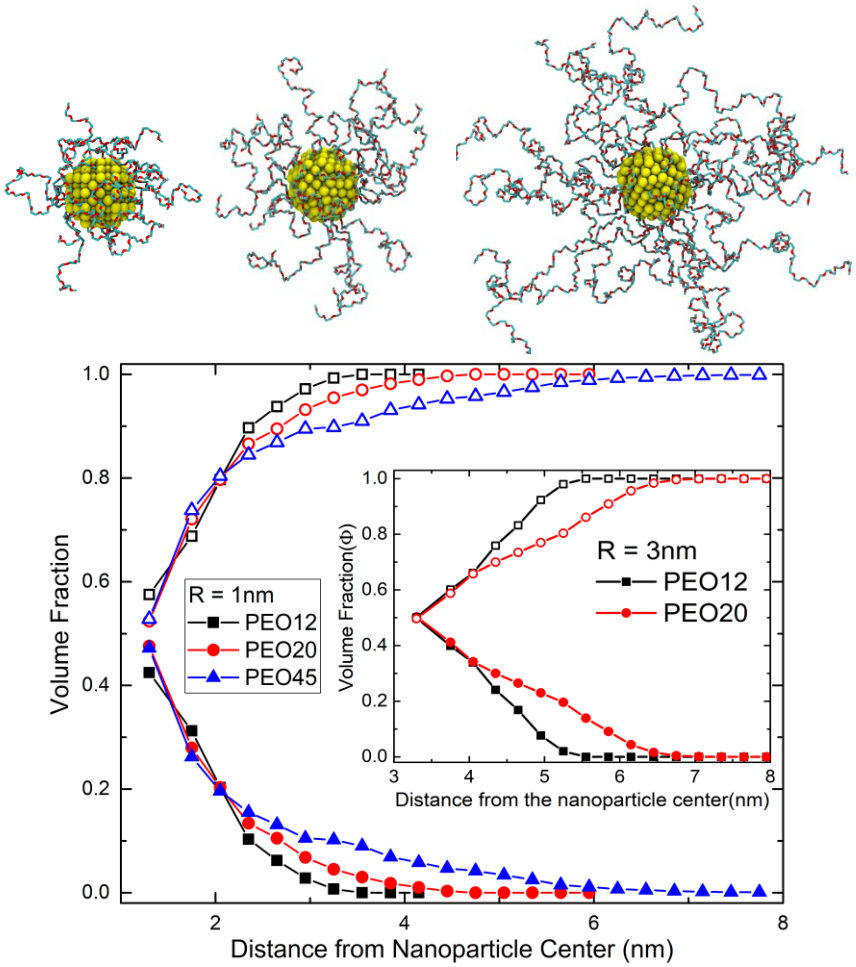

Figure 1. Computer simulation snapshots of 1nm gold nanoparticle grafted with PEO chains of 12, 20 and 45 repeat units. Grafting density, $\sigma = 1.5\ /nm^2$. Volume fractions of PEO (solid symbols) and water (open symbols) as a function of the radial distance from the center of the nanoparticle for PEO chains of different lengths: N=12 (black squares), 20 (red circles) and 45 (blue triangles) for gold nanoparticles of radius 1nm or 3nm (inset) at a grafting density of 1.5chains/nm^2. The snapshots were produced using VMD.[36]

Besides studying the overall polymer density profile, it is interesting to analyse the conformation of individual chains. As is seen from computer simulation snapshots there is some level of interactions (overlap) between different coils, at least for N=20 and 45, as is expected based on the average area per chain ~0.67nm^2 being smaller than R_{go}^2 for these chains, where R_{go} is the radius of gyration of the PEO chain in solution. Taking this into account, one would expect some degree of chain stretching at least near the nanoparticle surface and an increase in the overall chain size. However, this is not the case. Comparing the radius of gyration (and its components) for PEO chains (with N=12, 20 or 45) in solution and grafted to nanoparticles of 1nm with grafting density, $\sigma = 1.5\ /nm^2$ we found practically no difference at all, not only in the average values (see supporting information, Figure S3), but for distributions of principal axis of the radius of gyration as well (Figure S4). In Figure 2 the end-group distribution is compared for free PEO chain in solution and grafted to 1nm or 3nm gold nanoparticles (with grafting density, $\sigma = 1.5\ /nm^2$). As is seen distributions are virtually identical for PEO with 12 repeat units and only slightly shifted to larger values for PEO with 20 repeat units grafted to a 3nm nanoparticle. This is consistent with an experimental report[13] that the PEO layer thickness (obtained using DLS) on 15 nm Au nanoparticles with grafting densities exceeding 1/ R_{go}^2 is comparable to the PEO end-to-end distance in solution for a range of molecular weights (N from ca.47 to 1168), using the empirical scaling dependence relating molecular weight to the end-to-end distance.[37] In contrast, the end-to-end distance of PEO of 20 repeat units increased by 3.5 times when grafted to a planar surface with the same grafting density of $\sigma = 1.5\ /nm^2$ (see supporting information, Figure S3). This implies that the high curvature of small nanoparticles provides sufficient space to accommodate packing of polymer chains without a noticeable distortion of their shape. Interestingly, significant overlap of polymer coils at the surface does not necessary translate into chain stretching and brush-

like behaviour if nanoparticle curvature is high (at least for the range of studied chain lengths). This can have important implications for nanoparticle design: following a simple criterion of having grafting density exceeding 1/ R_{go}^2 and/or $1nm^{-2}$ does not guarantee a dense brush-like structure of PEO layer around a nanoparticle. A similar conclusion was made recently by Di Valentin et al. based on experimental and computer simulation data[12,14]. It has been also concluded that a grafting density well in excess of $1nm^{-2}$ is required to ensure sufficient nanoparticle surface shielding[2] and that PEO brush on small nanoparticle is more susceptible to protein adsorption at about $1nm^{-2}$ grafting density compared to PEO brush on planar surface.[8]

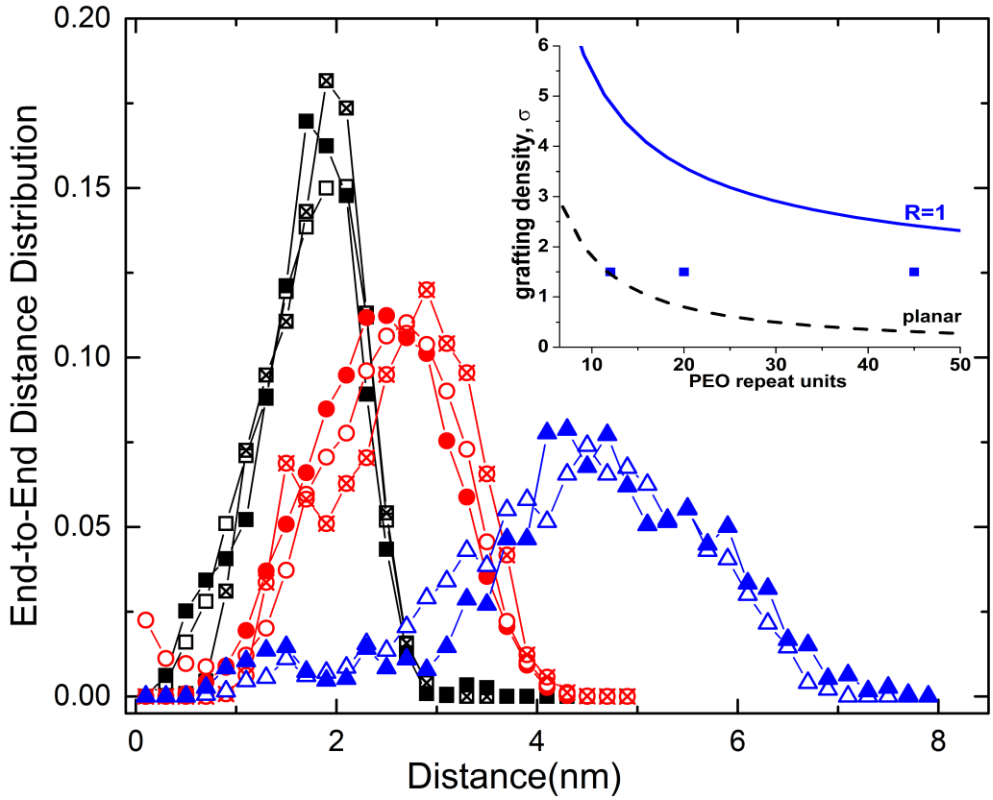

Figure 2. The end group distribution of PEO chains of 12 repeat units (squares), 20 repeat units (circles) and 45 repeat units (triangles) grafted to 1nm (solid symbols) or 3nm (crossed symbol) gold nanoparticles at grafting density $1.5 chains/nm^2$ in comparison to that for free chains in aqueous solutions (open symbols). The inset shows predictions of the theoretical model (eq.1)

(solid curve) for the polymer grafting density corresponding to the mushroom to brush transition for a spherical nanoparticle of 1nm in radius in comparison to that for planar surface (dashed curve) with data points showing the three molecular weights of PEO that we studied for nanoparticle of 1nm radius and grafting density $\sigma = 1.5\text{nm}^{-2}$.

In contrast to planar surfaces where the area per chain does not change with a distance from the surface, for spherical nanoparticles the area per chain increases as ~r^2 with the radial distance r. Thus, chain crowding on the nanoparticle surface does not necessary ensure coil overlap just above the surface. Therefore, it would be logical to allow for higher polymer density at the nanoparticle surface and consider the coil overlap at the distance of a coil radius above the surface, i.e. at $r=R+R_{go}$, where R is the core radius. This corresponds to the following condition:

$$4\pi\left(R + R_{go}\right)^2 = \pi R_{go}^2 Q \equiv 4\pi^2 R^2 \sigma R_{go}^2$$

leading to

$$\sigma^* \sim \left(\frac{1}{R} + \frac{1}{R_{go}}\right)^2 \qquad (1)$$

where Q is the number of chains grafted to a nanoparticle. In the limit of a flat surface, i.e. R→∞, we arrive to the usual $\sigma^* \sim 1/R_{go}^2$ for planar surfaces, while in the limit of very long polymer chain N→∞, $\sigma^* \sim 1/R^2$. Thus for very small nanoparticles it would require a rather high, perhaps unrealistic grafting density to achieve overlap at the distance of a coil radius above the surface, implying that the brush regime may not be reached.

Applying similar considerations for cylindrical nanoparticles we arrive at

$$\sigma^* \sim \frac{1}{R_{go}}\left(\frac{1}{R}+\frac{1}{R_{go}}\right) \quad (2)$$

which also recovers $1/R_{go}^2$ for planar surfaces and accounts for the cylindrical curvature effect, which has been considered in literature [38,39] As expected, in this case the curvature effect is weaker than for spheres, as the area available per chain expands linearly with radial distance, i.e. ~r. Predictions for the overlap grafting density are summarised in Table 1.

Table 1. Summary of predictions for the grafting density for the mushroom to brush transition.

Spherical surface	Cylindrical surface	Planar surface
$\sigma^* \sim \left(\frac{1}{R}+\frac{1}{R_{go}}\right)^2$	$\sigma^* \sim \frac{1}{R_{go}}\left(\frac{1}{R}+\frac{1}{R_{go}}\right)$	$\sigma^* \sim \frac{1}{R_{go}^2}$

Applying eq. 1 for a spherical nanoparticle of radius 1nm, as considered in Figures 1 and 2, we arrive at $\sigma^* \approx 6.2$ nm^{-2} for the grafting density required to see overlap at R_{go} height for PEO of 12 repeat units, $\sigma^* \approx 4.3$ nm^{-2} for PEO with N=20 and $\sigma^* \approx 2.8$ nm^{-2} for PEO with N=45, as is seen in the inset of Figure 2. Thus, for all chain lengths considered, we are in the mushroom regime, according to eq.1, which is consistent with the strong decay of the polymer volume fraction away from the surface (Figure 1) and the end-group distribution being nearly identical to the end-to-end distribution in solution (Figure 2). We note that for PEO of 20 repeat units attached to a gold nanoparticle of 3nm radius, $\sigma^* \approx 1.9$ nm^{-2} which is only slightly larger than considered here $\sigma = 1.5$ nm^{-2}, resulting in a slight deviation of the end group distribution towards larger distances as a result of chain overlap at the surface.

As we established that the PEO size and shape does not appreciably change upon grafting to nanoparticles at this moderate grafting density, it is interesting to investigate the level of polymer hydration. An analysis of hydrogen bonding with water (Figure S5 of supporting information) shows that except for the near vicinity of the gold surface the level of hydrogen bonding of PEO is the same as in solutions, i.e. close to 1.2 hydrogen bonds per repeat unit of PEO.[35] Similar observations have been made in recent computer simulations of PEO grated to TiO_2 nanoparticles.[12] Perhaps it is more informative to consider free water within the spherical shell of PEO, i.e. water which is not hydrogen bonded to PEO. Figure 3 shows radial dependence of the fraction of free water compared to total water at a given radial distance from the nanoparticle surface for PEO of different chain lengths grafted to 1nm and 3nm nanoparticles. As is seen, for PEO grafted to a 1nm nanoparticle the free water fraction remains below 0.5 within 1nm of the nanoparticle surface and is the same for PEO of different lengths. At larger radial distances the free water fraction quickly increases, which implies relatively easy water exchange and access to nanoparticle surface, where the free water fraction remains non-zero. For 3nm nanoparticles the free water fraction is lower, almost approaching zero at the nanoparticle surface and the region with a low fraction of free water is somewhat wider, indicating a somewhat larger polymer overlap within the nanoparticle corona.

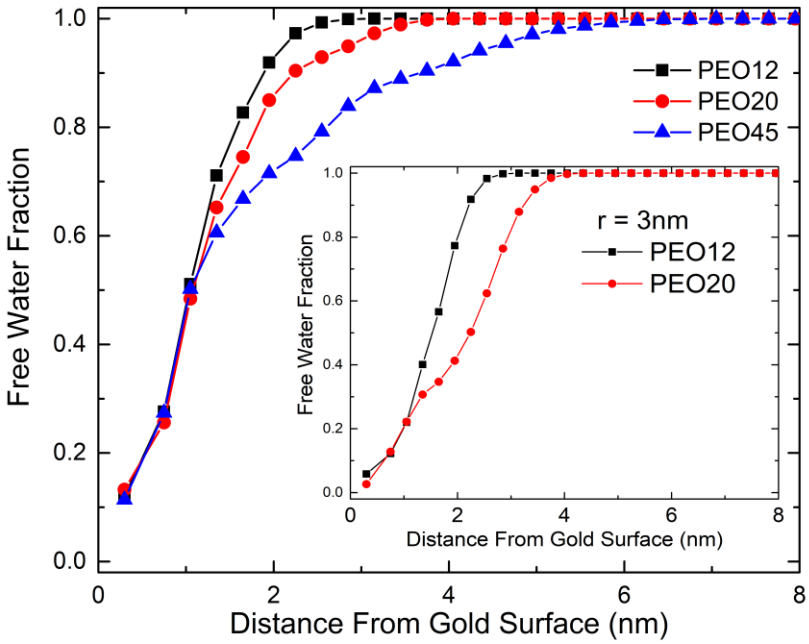

Figure 3. The average fraction of free water (e.g. fraction of water that is not hydrogen bonded to PEO) as a function of radial distance from the nanoparticle surface for PEO chains of different lengths N=12 (squares), 20 (circles) and 45 (triangles) for gold nanoparticles of radius 1nm or 3nm (inset) at grafting density of 1.5chains/nm^2.

Thus, at a moderate grafting density PEO chains grafted to a gold nanoparticle of high curvature maintain the same size and shape as in solution with the polymer density decreasing in an exponential-like manner away from the surface. The polymer density and hydration near the surface does not change with polymer length and indicates some level of overlap, but does not reach the brush regime, even when the average distance between grafting sites is less than R_{go}. At this grafting density accessibility of water to the nanoparticle surface remains high.

High grafting density. At a high grafting density of $\sigma = 4.18\ /nm^2$ polymer chains are in the brush regime, as is seen in a cross-sectional view of computer simulation snapshots shown in Figure 4 for PEO chains of lengths N=12, 20, 36 and 45. In the vicinity of the gold surface the polymer conformation and brush structure is rather similar in all cases and obviously grafting longer PEO chains to a gold nanoparticle results in spherical brushes of increased thickness. As will be discussed in more detail below, we observe a dense polymer-dominated zone near the gold surface and a more diffuse better hydrated outer shell. Qualitatively similar dense and semi-dilute regions of spherical polymer brushes were observed using SANS and SAXS measurements for gold and iron oxide nanoparticles of comparable sizes[27,28,40] as well as silica nanoparticles of a larger size.[41,42]

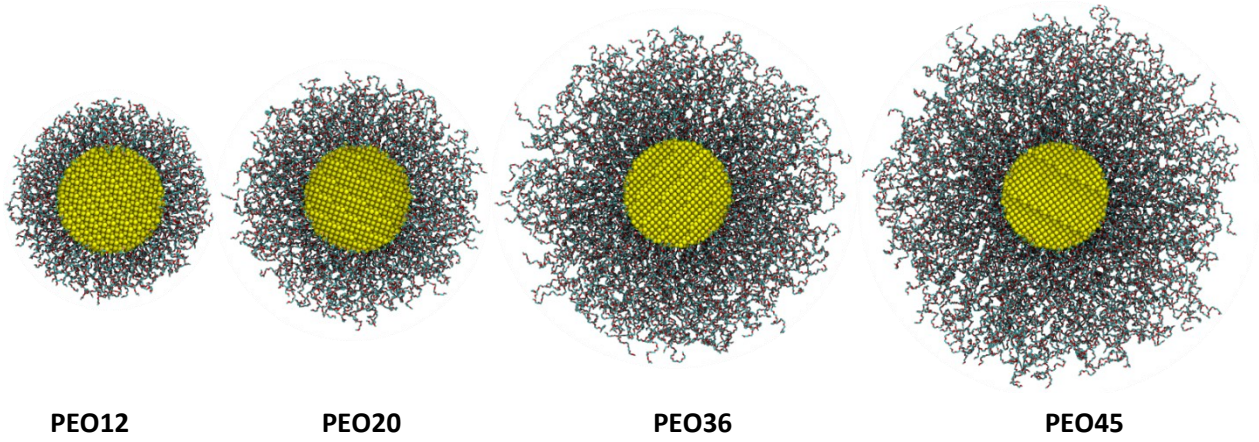

Figure 4. Cross-sectional computer simulation snapshots of the gold nanoparticles grafted with PEO chains of different chain lengths: N=12, 20, 36 and 45. Gold nanoparticle is shown in yellow, PEO chains in cyan (carbons) and red (oxygen). PEO hydrogens and water are not shown for clarity. Gold nanoparticle radius is 3nm and grafting density, $\sigma = 4.18\ /nm^2$ in all cases.

We analyzed the spherical brush structure and calculated the volume fractions of PEO and water in the nanoparticle shell, which are shown in Figure 5 as functions of the radial distance from the

nanoparticle center of mass. As is seen, the volume fraction of PEO reaches about 0.7 in the immediate vicinity of the gold surface, which is to be expected for the high grafting density studied here. In general, a high volume fraction of PEO near the gold core can in part be a result of PEO adsorption on gold[20,21,24] to substitute for layered water[43], but this effect should be rather small taking into account the high grafting density considered. Comparing results obtained for PEO chains of different lengths as shown in Figure 5, one can notice that all volume fraction profiles coincide within 2-2.5nm of the gold surface. This reflects the observation made from the snapshots shown in Figure 4 that in all cases the PEO layer structure looks practically identical near the gold surface. Inside the 2nm wide spherical zone near the gold surface the PEO volume fraction exceeds that of water (Figure 5) and PEO is dehydrated, as will be discussed below. A similar observation of a dense PEO region within ~1.7 nm of the surface of a spherical gold nanoparticle was made by Lennox et al.[27] and based on SANS data fitting indicated nearly 0.93 volume fraction for PEO in this region for 2.5nm radius gold nanoparticles with an estimated PEO grafting density of $\sigma \sim 7\ to\ 7.9 nm^{-2}$. A dense (constant density) spherical PEO layer of $1 \pm 0.2\ nm$ was also experimentally observed[28] near the surface of spherical iron oxide nanoparticles of $3.7 \pm 0.4\ nm$ diameter for PEO grafting density $\sigma \sim 3.5\ nm^{-2}$. Further away from the gold surface the PEO volume fraction starts to decline at different radial distances from the gold nanoparticle centre depending on the PEO chain length (Figure 5). In this outer shell the water volume fraction dominates and PEO is expected to be well-hydrated, at least as in the semi-dilute regime.

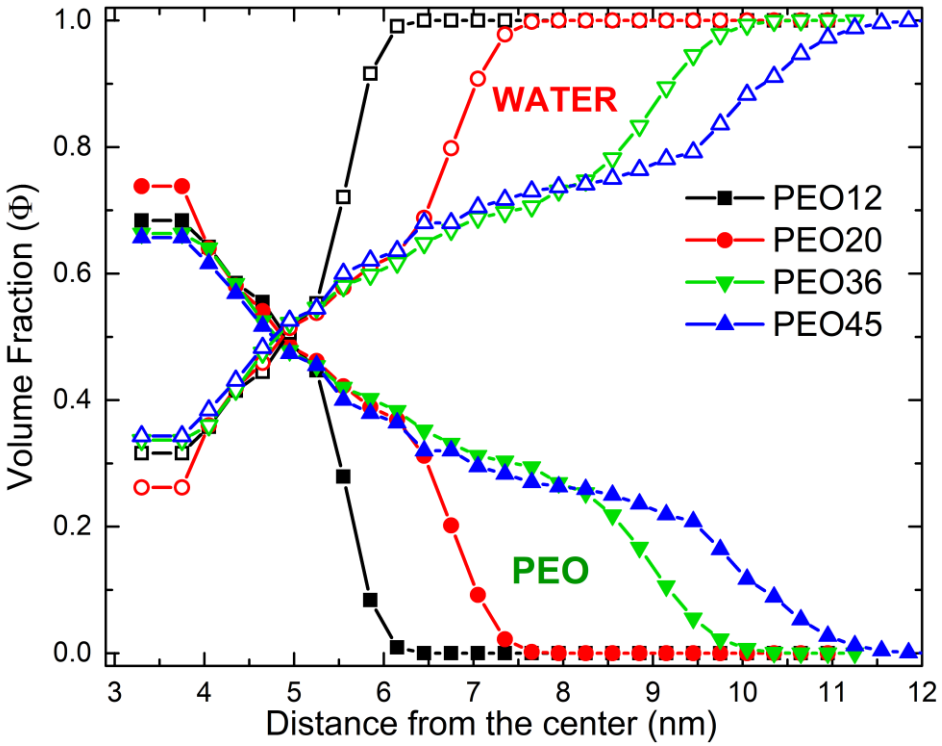

Figure 5. Volume fractions of PEO (solid symbols) and water (open symbols) in the spherical shells of gold nanoparticles as functions of the radial distance from the center of the nanoparticle for PEO chains of different lengths: N=12 (black squares), 20 (red circles), 36 (green down triangles) and 45 (blue up triangles). The gold nanoparticle radius is 3nm and grafting density $\sigma = 4.18\ /nm^2$.

It is informative to plot the radial dependence of PEO volume fraction in spherical shells of nanoparticle in logarithmic scale, as shown in Figure 6. As is seen, the volume fraction profiles obtained for different PEO lengths coincide with each other and follow the same scaling dependence, except for the periphery of the polymer shell where polymer end-groups are located. Similar trends have been reported in generic MD and DFT calculations.[44] The most commonly

used scaling model for polymer stars, micelles and polymer grafted spherical nanoparticles is the Daoud-Cotton model[45] and its modifications and improvements[46–48] which all lead to

$$\Phi(r) \propto r^{-\frac{4}{3}} \qquad (3)$$

for the semi-dilute regime expected for polymer corona in a good solvent, where $\Phi(r)$ is the volume fraction and r is the distance from the centre of nanoparticle. Similar to experimental observations and simulation results for generic polymers[28,38,44] we indeed find that our results follow this expected scaling. It is interesting to note that even in the first zone closest to the gold surface, i.e. at $r \leq 5.5nm$, where the PEO volume fraction dominates and can be viewed as a concentrated regime, the scaling remains the same. We do not observe $\Phi(r) \propto r^{-1}$ expected for the concentrated regime[45], nor do we see a constant density $\Phi(r) \approx const$ in the dense PEO region as has been used to fit experimental scattering data.[27,28] We believe that the disagreement with the theoretically expected[45] scaling $\Phi(r) \propto r^{-1}$ arises from chain stretching and orientation, which is not accounted for theoretically, but does occur in the nanoparticle surface vicinity, as we will discuss next.

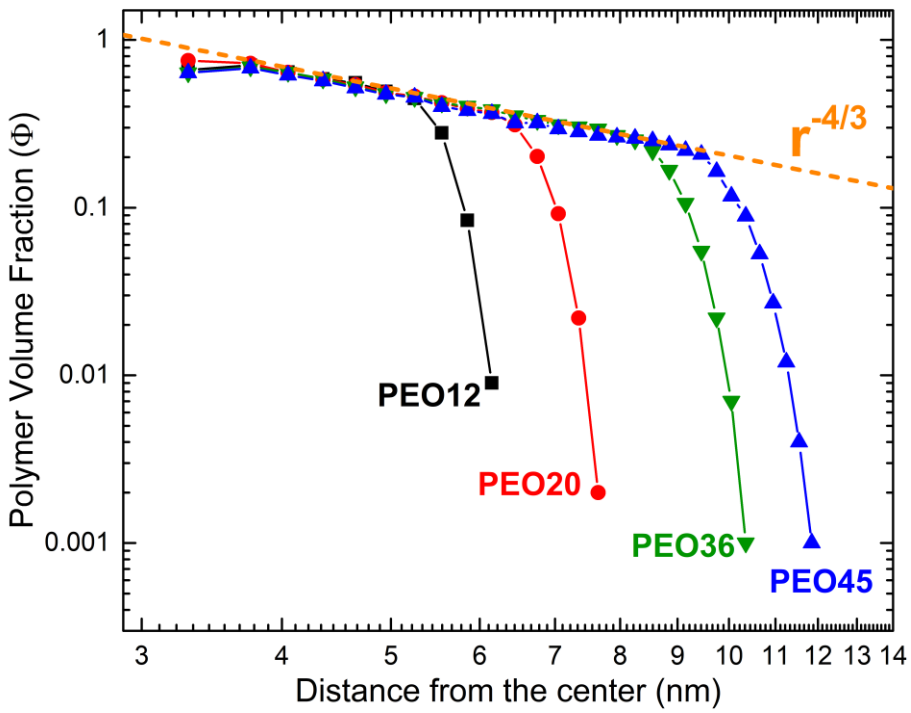

Figure 6. Volume fractions of PEO in the spherical shells of gold nanoparticles as functions of the radial distance from the center of the nanoparticle plotted in a double logarithmic scale for PEO chains of different chain lengths: N=12 (black squares), 20 (red circles), 36 (green down triangles) and 45 (blue up triangles) in comparison with the analytical scaling of eq.3 (dashed line).

To characterize the local PEO chain stretching in the spherical shell, we calculated the ratio $\alpha^2 = < r_s^2(r) > / < r_{so}^2 >$ of the square of oxygen-to-oxygen separation distance r_s along the PEO chain (averaged among all chains and over 500 frames) in a given radial shell to that obtained for free PEO chain of the same length in dilute solution $< r_{so}^2 >$ ($< r_{so}^2 >= 0.0784 nm^2$). The results are shown in Figure 7a as a function of radial distance r from the nanoparticle centre. As is seen, PEO chains are most stretched near the gold surface, as expected, even though the extent of stretching is not so large. Local chain stretching is rather similar for PEO chains of different molecular

weights. Chain stretching dissipates approximately at 5-5.5nm from the nanoparticle centre (i.e. 2-2.5nm from the gold surface), which coincides with the boundary of the dense PEO zone, shown in Figure 5. At larger radial distances no appreciable stretching is observed.

Local chain stretching near the gold surface is obviously caused by chain crowding which should also lead to preferable chain orientation away from the surface. To quantify local chain orientation, we calculated the orientational order parameter:

$$S(r) = 0.5 < (3Cos^2\theta - 1) > \qquad (4)$$

for oxygen-to-oxygen vectors along the PEO chain (starting from the oxygen closest to the gold surface) with respect to radial vector (drawn from nanoparticle centre to the grafting point of the chains) with θ being the angle between these two vectors. The average is taken among all chains attached to the nanoparticles and over 500 frames. The obtained orientational order parameter S(r) is shown in Figure 7b for different PEO chain lengths. The order parameter behaves in a very similar manner in all cases and as is seen, PEO chains are noticeably oriented in the vicinity of the gold surface with the order parameter approaching 0.6. As the distance from the surface increases the preferential orientation along the radial direction diminishes and approaches S(r)≈0.2 at the boundary of dense PEO zone. It is interesting to note that the rate of the orientational parameter S(r) decline changes at this point, i.e. at approximately 5-5.5nm distance from the nanoparticle centre (i.e. 2-2.5nm from the gold surface). At large radial distances from the gold surface the orientational order continues to decline, but at a slow rate until it disappears. Comparing OCCO dihedral distributions for the sections of PEO chains in the dense region near the gold nanoparticle surface and at the periphery of grafted PEO layer (Figure S6 of supporting information), one can notice enhancement of the trans conformation near the nanoparticle surface, which is consistent

with the chain stretching and orientation shown in Figure 7, as well as with dehydration in this region, which will be discussed below. Thus, comparing Figures 5,6 and 7, we can conclude that higher PEO grafting density leads to chain stretching and orientation within 2-2.5nm of the gold surface, but it does not manifest itself in r^{-1} scaling dependence as $\Phi(r) \propto r^{-4/3}$ remains valid even in this zone.

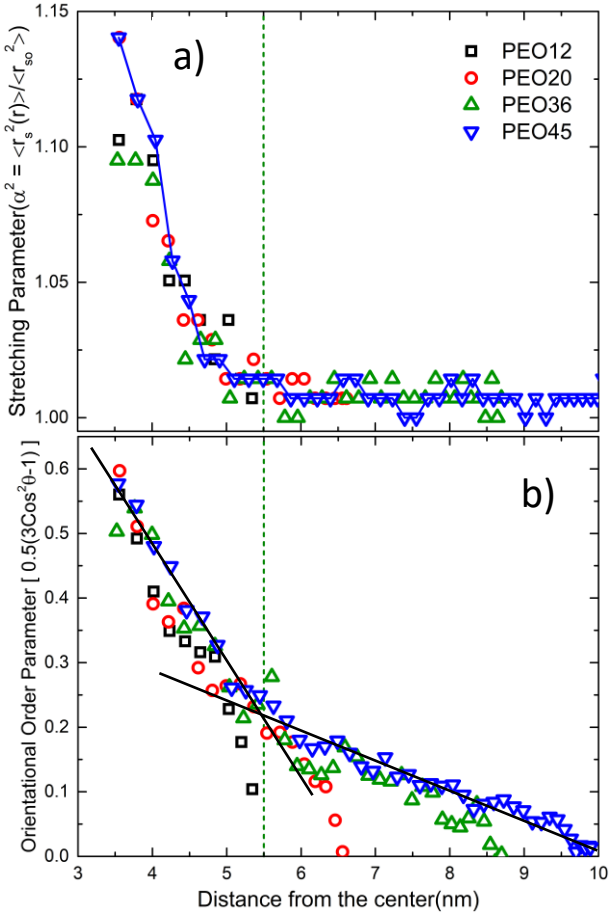

Figure 7. Local chain stretching parameter $\alpha^2(r)$ (a) and the orientational order parameter S(r), eq.4 (b) as functions of the radial distance from the center of the nanoparticle for PEO chains of different chain lengths: N=12 (black squares), 20 (red circles), 36 (green up triangles) and 45 (blue down triangles). Two different slopes for the orientational order parameters are shown as thin straight lines. The boundary of the dense PEO zone is marked by the vertical dashed line.

Accounting for chain stretching, e.g. using the approach of ref.46, results in the familiar $\Phi(r) \propto r^{-4/3}$ scaling even in the theta-solvent or polymer melt regime near the surface, as is seen in Figure 6. Thus, the observed $\Phi(r) \propto r^{-4/3}$ scaling dependence does not necessarily imply a good solvent condition or swelling of polymer inside the polymer corona. While we observe some chain stretching near the interface, Figure 7a, it seems to be independent of chain length. From the orientational order analysis we can see some increased orientation of the polymer chains near the gold surface. To test the end group exclusion zone as suggested by Dan and Tirrell,[48] we calculated end group distributions (Figure S7 in supporting information) for the spherical shells of PEO of different lengths. For all cases, we see an exclusion zone, which increases with the chain length: for PEO12 the exclusion zone is $\sim 1.5\ nm$, for PEO20 it increases to $\sim 2nm$, for PEO36 $\sim 3.5nm$ and for PEO45 $\sim 4nm$. The origin of the exclusion zone is the existence a strong steric repulsion between PEO chains near the gold surface, which depends on PEO grafting density and makes this area of high polymer concentration less penetrable for the end groups. This behaviour is in contrast to what we observed for moderate grafting densities (Figure 2) where no exclusion zone is observed and end-group distribution was rather similar to that in solution.

Chain stretching and orientation away from nanoparticle surface have important implications regarding the brush height. To further characterize the effect of chain orientation and stretching on the overall chain dimensions in the brush, we calculated the end-to-end distance and radius of gyration for different chain length in the spherical brush and compare to solution values (Table S2 in supporting information). We find that the end-to-end distance for a chain in the spherical brush exceeds that in solution by more than 1.5 times as shown in the inset of Figure 8 and R_g exceeds

the solution values by more than ~1.3times. This indicates that chain orientation and stretching have significant impact on brush height as expected for high grafting density.

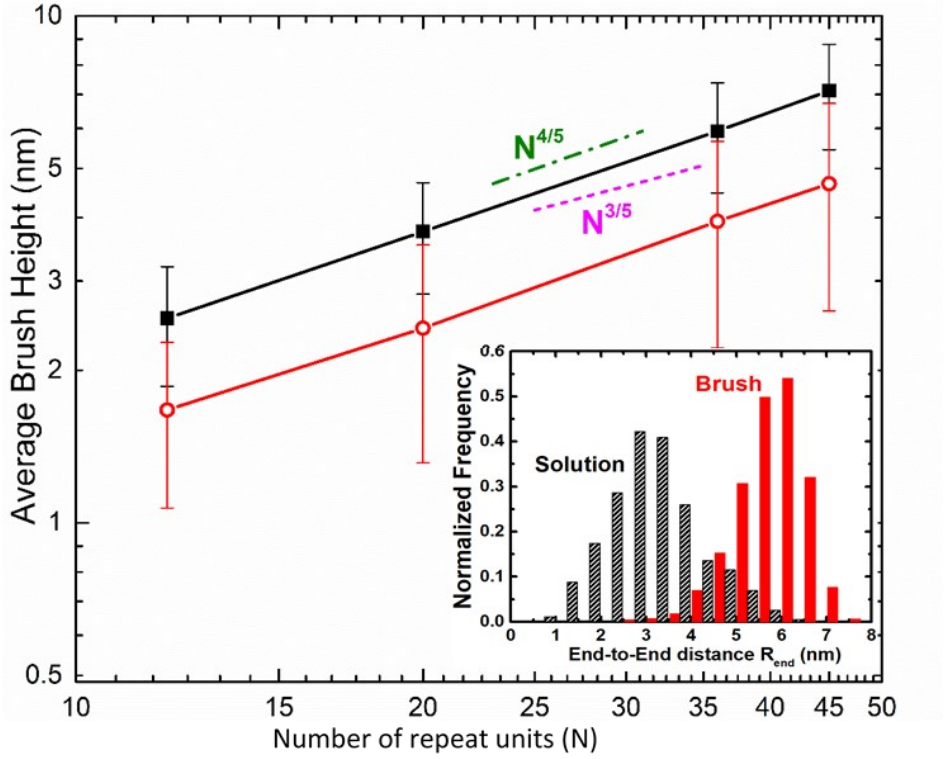

Figure 8: Average brush height calculated using eq.5 (open symbols) and by analysing end-group distribution (solid symbols) as a function of the number of PEO repeat units. The dashed line shows $N^{\frac{3}{5}}$ dependence whereas dash-dot line shows $N^{\frac{4}{5}}$ scaling. The inset shows the end-to-end distance distribution for PEO36 chain in water (striped grey bar) and PEO36 chain in a spherical brush (red solid bar). Gold nanoparticle radius is 3nm and grafting density, $\sigma = 4.18\ /nm^2$.

We calculated the average height of the spherical brush as second moment of density profile defined as[49,50]

$$H_{avg}^2 = \int_R^\infty r^2 dr\ \Phi(r)(r-R)^2 / \int_R^\infty r^2\ dr\ \Phi(r), \qquad (5)$$

where R is core radius, r is the distance from the centre of the gold nanoparticle. Figure 8, shows in a logarithmic scale the brush height as a function of chain length N. The line with open symbols represents the average brush height obtained using eq. 5, while the line with solid symbols is the average brush height estimated from the end group distribution (Figure S7 in supporting information) taken as the position of the maximum of the distribution. As is seen, the estimation of brush height from the end group distribution yields a systematically somewhat higher value than obtained using eq.5, which is not unexpected as these two definitions are based on different brush properties. More importantly both definitions result in a similar scaling dependence. In general, there is an established notion that the average height of a spherical surface scales as $H_{avg} \cong \sigma^{\frac{1}{5}} N^{\frac{3}{5}} R^{\frac{2}{5}}$ in the semi-dilute regime[45,47] and can achieve $H_{avg} \sim N$ in a concentrated regime (in the absence of swelling by solvent).[9,51] Our results shown in Figure 8 seems to follow somewhat stronger dependence than $N^{\frac{3}{5}}$, more like $N^{\frac{4}{5}}$, even though we note the large error-bars in brush height estimations. Computer simulation data obtained by generic MD and self-consistent DFT analysis also show somewhat stronger than $N^{3/5}$ scaling for a polymer star, which follows a $N^{\frac{2}{3}}$ dependence.[38,44] Experimentally a $N^{\frac{4}{5}}$ scaling dependence for the brush height was reported for polystyrene-grafted silica particles of $14 \pm 4\ nm$ diameter [41] and $N^{0.83}$ scaling has been observed for high molecular weight poly(methyl methacrylate) (PMMA) chains grafted on silica nanoparticle with core radius 2.5nm.[9] In both cases grafting densities were around 1 nm^{-2}. Thus, our results show, in agreement with experimental data, that at high grafting densities chain stretching and orientation results in a dense polymer area near the nanoparticle interface leading to a brush height increase with chain size exceeding that expected for the semi-dilute regime.

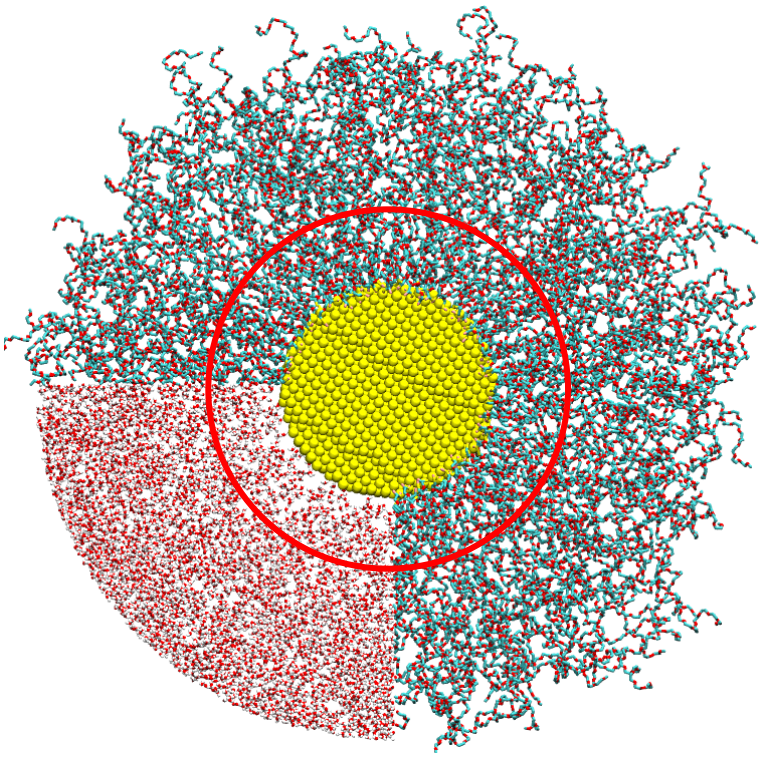

Figure 9: Cross-sectional view of a PEO45 brush illustrating the two-shell model. The circle(red) indicates the $\sim 2\ nm$ radius dehydrated region. We removed PEO from bottom left 1/4th portion and water and PEO hydrogens from the remaining 3/4th portion for clarity. The central region (yellow beads) represents the gold nanoparticle. Gold nanoparticle radius is 3nm and grafting density, $\sigma = 4.18\ /nm^2$.

Having discussed conformational properties of PEO in a spherical layer, it is worthwhile to look at the polymer hydration. Figure 9 shows the cross-sectional view of PEO45 spherical brush and water inside the brush. As is seen, near the gold surface, where the polymer is stretched and oriented, the water concentration is rather low. Accordingly, the degree of hydrogen bonding between the polymer and water is very low, about 0.5-0.6 water molecules per repeat unit of PEO, i.e. half of the solution level (Figure 10a). We note that in this region all available water is hydrogen bonded to PEO, so no free water can be found (Figure 10b). Farther away from the

surface the water concentration increases, while the polymer orientation dissipates and the degree of hydrogen bonding increases as well. At radial distances exceeding 2-2.5nm from the gold surface the free water level stabilizes and hydrogen bonding reaches the bulk values (Figure 10a). We note that the hydration shell of PEO remain incomplete at about 2 water molecules per PEO repeat unit at 2nm radial distance from the gold surface, (Figure S8, supporting information) as the fraction of free water remains very low at that distance (Figure 10b). Thus, with respect to water distribution in the spherical shell, one can separate the inner shell of low hydration r<5nm where the polymer is present at high concentration, stretched and oriented along the radial direction and the outer shell r≥5nm where the polymer is more hydrated, maintaining solution level degree of hydrogen bonding, but with less than complete hydration shell. This subdivision into the zones remains valid for a given high grafting density independently of the chain length, since the hydration of polymer brushes is mainly independent of chain length (Figure 10, Figure S8 of supporting information). The observed difference in hydration in the inner and outer shells is consistent with experimental observations for polymer-grafted nanoparticles.[27,28] Experimentally, Lennox et. al. analysed SANS data for PEO capped gold nanoparticles using a two-shell model with an inner shell of about $\sim 1.7nm$ containing nearly completely dehydrated PEO (93% by volume) and an outer hydrated shell with almost 60% of PEO by volume.[27] We note that PEO of 45 repeat units was attached to a gold nanoparticle of $\sim 2.5\ nm$ radius at a rather high grafting density $\sigma \sim 7\ to\ 7.9nm^{-2}$ far exceeding what we used in our simulations, $\sigma \sim 4.18nm^{-2}$. Recent scattering experiments on PEO (Mw=5000Da) grafted iron-oxide nanoparticle of 3.7 nm radius with a grafting density of 3.5nm^{-2} also invoke a core-shell model with a constant density profile for the concentrated brush regime within ~1nm of nanoparticle surface.[28] While the width of the low hydration zone is mainly independent of molecular weight, it is strongly influenced by

polymer grafting density and nanoparticle curvature, as discussed in our previous publication.[20] Using atomistic molecular dynamics simulations we have shown that the low hydration zone increases from a few angstroms for small nanoparticles with low polymer grafting density to 2-2.5nm at high grafting density and larger nanoparticle size and can reach 5.5nm for a planar PEO brush of high density $\sigma = 4.18\ /nm^2$.[20]

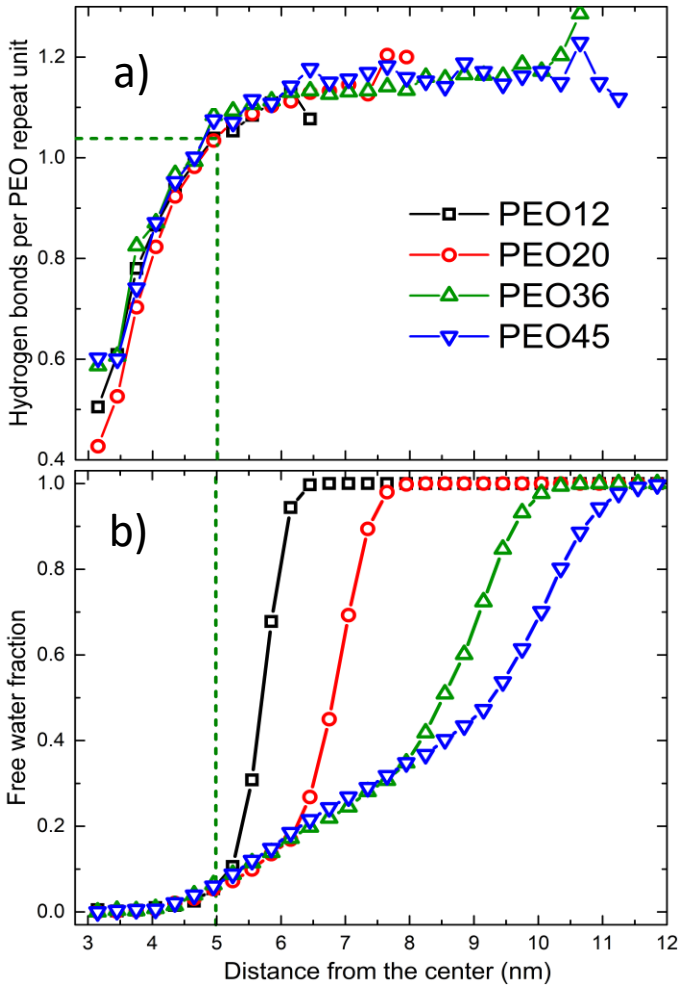

Figure 10: a) The average number of hydrogen bonds with water per repeat unit of PEO; b) the average fraction of free water that is not hydrogen bonded to PEO as functions of radial distance from the gold nanoparticle centre. Vertical dashed line indicates the boundary of the dense and

partially dehydrated PEO region. Gold nanoparticle radius is 3nm and grafting density, $\sigma = 4.18\, nm^{-2}$.

To investigate the dynamics of PEO chains within the spherical brush we monitored changes in polymer conformations as a function of time. Figure 11a shows the series of time trajectory snapshots of PEO chain conformations within spherical brushes of different sizes obtained during a 1ns time period for one of the representative chains from each polymer brush. As is seen, within about 2nm from the gold surface the PEO chain conformation remains rather stagnant and similar for all PEO chain lengths considered. This is consistent with the chain stretching and orientation within this dense inner shell discussed above which does not contain free (unbound water). For the shortest chain length studied, N=12, the inner zone represents the majority of the shell, so only the chain tails are mobile and significantly change conformation with time. With an increase of PEO chain length the fraction of the inner dense zone diminishes and we start to observe variation in the chain conformation within the outer shell. This variation becomes more pronounced with an increase in chain length and in all cases the very ends of the PEO chains exhibit the maximum mobility. To characterize the chain tail flexibility we calculated the time dependent orientational order parameter C_{tail} for oxygen-oxygen vector for last three monomers of the chain tail using subsequent time frames:

$$C_{tail}(t) = \langle \frac{1}{2}(3\,\mathrm{Cos}^2\,\theta - 1) \rangle \qquad (6)$$

where $Cos\theta = [\vec{r}_i(0).\vec{r}_i(t)]/|\vec{r}_i(0)||\vec{r}_i(t)|$ and $\vec{r}_i(t)$ is the three segment tail vector at time t, as shown in the Figure 11b and $\vec{r}_i(0)$ is the vector at t=0 . This function goes to zero when there is no correlation with the original orientation of the chain tail. The obtained time-dependent

orientational order parameter C_{tail} is shown in Figure 11b. We find that for longer chains the initial tail orientation dissipates within 0.5ns, while for shorter chains correlation with initial orientation persists over 1ns time range. The mobility of PEO chain is considered to be one of the important factors in preventing protein adsorption.[2,17,24–26,52] The results shown in Figure 11 indicate that longer chains retain higher mobility that is preferable for prevention of protein adsorption.

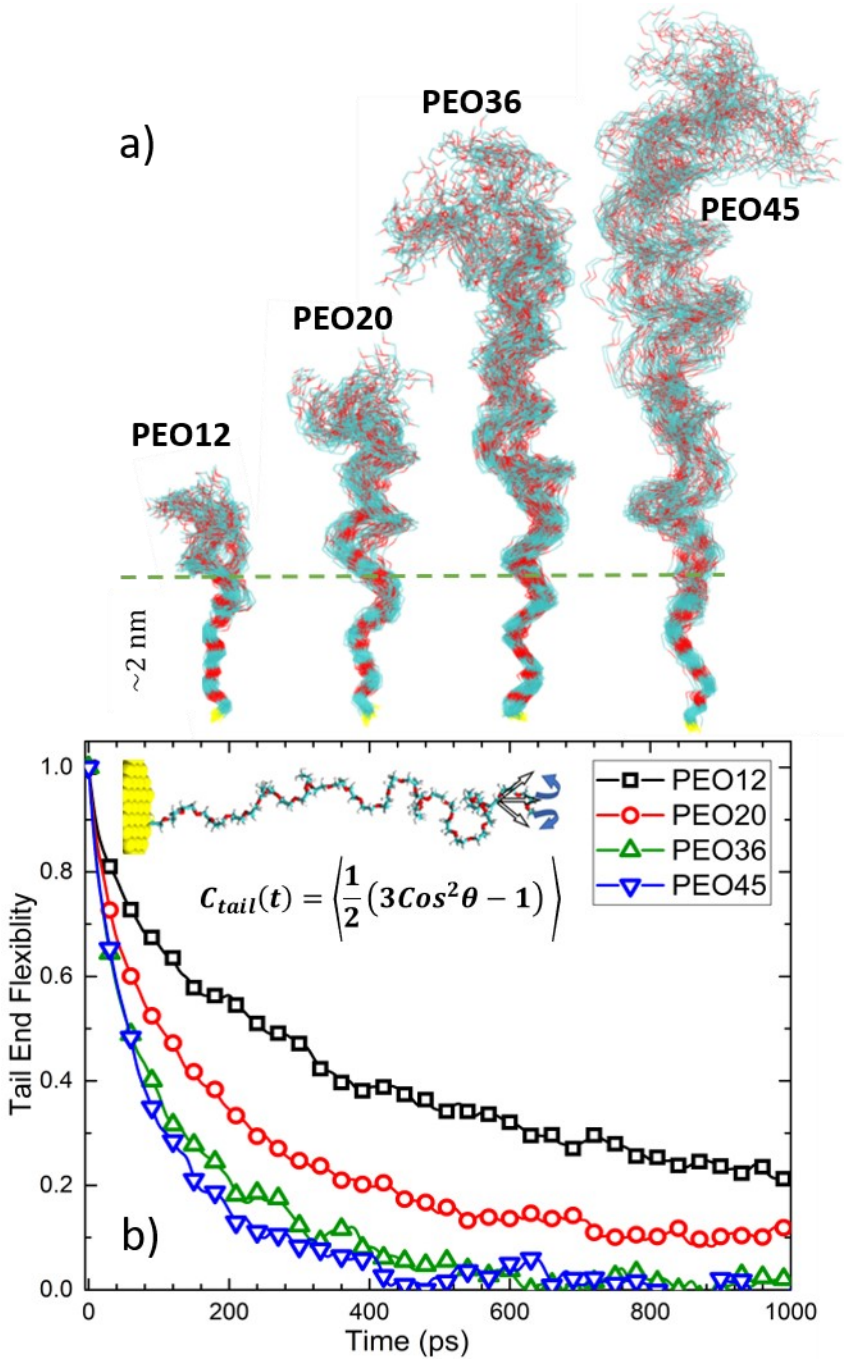

Figure 11 a) Computer simulation snapshots of PEO chain conformation recorded over 1ns time evolution trajectory for PEO of 12, 20, 36 and 45 repeat units in a spherical polymer brushes. b) Tail end flexibility autocorrelation function C_{tail}(t) for PEO chains of different length N=12, 20, 36 and 45 in a spherical brush. Gold nanoparticle radius is 3nm and grafting density, $\sigma = 4.18\, nm^{-2}$. The inset in 11b shows PEO chain snapshot with a vector along the last three tail monomers used to calculate the tail end flexibility.

Polymer hydration is another factor affecting protein adsorption.[2,18,24] As discussed above, the dehydration zone is practically independent of chain length for the high grafting density considered here. For shorter PEO chains the contribution of inner less hydrated zone to the overall shell is larger, the PEO chains are effectively less hydrated and less mobile. Thus, not only the tail flexibility but also the overall hydration of the shell and dynamics of hydrating water in the shell depend on the chain length with longer PEO chains being beneficial in protecting nanoparticle, maintaining a high water content in the shell and chain tail flexibility that can be favorable in preventing protein adsorption.[2,7,18,53]

Conclusions

Using atomistic molecular dynamics simulations we investigated polymer conformation and hydration of PEO layers grafted to spherical nanoparticles of 1-3nm radius at moderate (1.5 nm^{-2}) and high (4.2nm^{-2}) grafting densities for different PEO lengths. We found that at moderate grafting density the polymer conformation remains rather similar to that in solution, at least for the polymer lengths studied, despite polymer overlap at the nanoparticle surface. This indicates that the

mushroom to brush criterium for planar surfaces $\sigma^* \sim 1/R_{go}^2$ does not ensure achievement of an actual brush structure when chains are attached to small nanoparticles of high curvature because the radially increasing (away from the surface) available space allows enough freedom to accommodate the preferable chain conformations similar to dilute solution. Polymers remain well-hydrated within the layer with a decrease in the fraction of free water only close to the surface. To achieve a consistent polymer coverage of the nanoparticle surface, one may require polymer overlap not only at the surface, but at height R_{go}, which leads to modified estimate for the required grafting density to achieve the brush regime, $\sigma^* \sim (1/R_{go}+1/R)^2$ for spherical nanoparticles of radius R, which accounts for both the curvature of the nanoparticle and polymer coil dimension. Similar consideration can be applied to cylindrical surfaces, as summarized in Table 1. These expressions recover the mushroom-to brush criterium for planar surfaces and predict that for nanoparticles, of high curvature an increasingly large grafting density is required to achieve the brush regime, which is important to ensure nanoparticle shielding and inhibition of protein adsorption.[2,18,24]

For a densely grafted PEO layer we observe highly oriented, stretched and dehydrated PEO (with practically no free water) within 2nm of the gold nanoparticle surface independent of the PEO chain length. Further away from the surface the PEO layer become disoriented and more hydrated. For the whole width of the spherical layer, including the dense area near the nanoparticle surface, the PEO density decreases following a $\sim r^{-4/3}$ dependence, as expected based on the Daoud-Cotton model and observed experimentally.[28,45] In contrast to experimental data interpretations we do not observe a constant density area or $\sim r^{-1}$ dependence for the polymer density near the nanoparticle surface. Chain orientation and stretching in this area show that a model of screened volume interactions near the surface may not be valid for densely grafted nanoparticles, but rather an

oriented stretched brush needs to be considered. The overall polymer layer height follows a $N^{4/5}$ rather than the expected $N^{3/5}$ dependence, similar to what was observed experimentally and reported in (generic MD or MC) simulations. [9,38,41,44] The structural properties of the spherical layers formed by PEO of different lengths coincide within a certain distance from the gold surface with the largest difference in the chain tail flexibility. For the shortest PEO chain length considered, chain orientation persists throughout the whole layer, resulting in low flexibility of the tails. With an increase in chain length the orientation starts to dissipate with tails becoming more flexible at the periphery of the layer and above some length tail flexibility starts to achieve that found in dilute solution.

The obtained results show that the curvature of nanoparticles and grafting density both play an important role in determining hydration and structural properties of PEO spherical brushes. Closer to the nanoparticle surface the brush properties are nearly independent of the PEO length, but the flexibility of chain ends may depend on it. We suggest a modified criterion for achieving the brush regime for curved nanoparticles, which can be used to guarantee sufficient chain overlap within the grafted polymer layers. The obtained insights on hydration, chain conformation and mobility of PEO chains in grafted spherical layers can guide experimental exploration and technological development of polymer-grafted nanoparticles for biomedical applications.

Corresponding Author:

Email: elena@uconn.edu

Acknowledgements: This research is supported by the National Science Foundation under Grants No. DMR-1410928 and DMR-1916864.

Supporting Information: Computer simulation details for backmapping and equilibration; the end-to-end distance, radius of gyration and the aspect ratio for PEO chains of different lengths in aqueous solutions; comparison of Rg and end-to end distance for PEO chains grafted to nanoparticles at grafting density $1.5nm^{-2}$ to that in solution; distributions for the principle axis of the radius of gyration for PEO of 45 repeat units grafted to 1nm nanoparticle with grafting density $\sigma = 1.5$ nm^{-2}; average number of hydrogen bonds with water per repeat unit of PEO chains of 12 and 20 repeat units grafted to 1 and 3nm gold nanoparticle at grafting density of $1.5nm^{-2}$; dihedral angle distribution for OCCO dihedrals near the gold surface and away from it for PEO36 and PEO45 grafted to spherical gold nanoparticles (R=3nm) at grafting density $\sigma = 4.2nm^{-2}$; end group distribution, water hydration for PEO chains grafted to 3nm gold nanoparticles at grafting density of $\sigma = 4.18nm^{-2}$.

References:

(1) Jokerst, J. V.; Lobovkina, T.; Zare, R. N.; Gambhir, S. S. Nanoparticle PEGylation for Imaging and Therapy. *Nanomedicine* **2011**, *6* (4), 715–728. https://doi.org/10.2217/nnm.11.19.

(2) Suk, J. S.; Xu, Q.; Kim, N.; Hanes, J.; Ensign, L. M. PEGylation as a Strategy for Improving Nanoparticle-Based Drug and Gene Delivery. *Adv. Drug Deliv. Rev.* **2016**, *99*, 28–51. https://doi.org/10.1016/j.addr.2015.09.012.

(3) Cruje, C.; Chithrani, D. B. Polyethylene Glycol Functionalized Nanoparticles for Improved Cancer Treatment. *Rev. Nanosci. Nanotechnol.* **2014**, *3* (1), 20–30. https://doi.org/10.1166/rnn.2014.1042.

(4) Verimli, N.; Demiral, A.; Yılmaz, H.; Çulha, M.; Erdem, S. S. Design of Dense Brush Conformation Bearing Gold Nanoparticles as Theranostic Agent for Cancer. *Appl. Biochem. Biotechnol.* **2019**, *189* (3), 709–728. https://doi.org/10.1007/s12010-019-03151-6.

(5) Rabanel, J. M.; Hildgen, P.; Banquy, X. Assessment of PEG on Polymeric Particles Surface, a Key Step in Drug Carrier Translation. *J. Control. Release* **2014**, *185* (1), 71–87. https://doi.org/10.1016/j.jconrel.2014.04.017.

(6) Etame, A. B.; Smith, C. A.; Chan, W. C. W.; Rutka, J. T. Design and Potential Application of PEGylated Gold Nanoparticles with Size-Dependent Permeation through Brain Microvasculature. *Nanomedicine Nanotechnology, Biol. Med.* **2011**, *7* (6), 992–1000. https://doi.org/10.1016/j.nano.2011.04.004.

(7) Chithrani, D. B. Polyethylene Glycol Density and Length Affects Nanoparticle Uptake by Cancer Cells. *J. Nanomedicine Res.* **2014**, *1* (1), 1–6. https://doi.org/10.15406/jnmr.2014.01.00006.

(8) Gal, N.; Schroffenegger, M.; Reimhult, E. Stealth Nanoparticles Grafted with Dense Polymer Brushes Display Adsorption of Serum Protein Investigated by Isothermal Titration Calorimetry. *J. Phys. Chem. B* **2018**, *122* (22), 5820–5834. https://doi.org/10.1021/acs.jpcb.8b02338.

(9) Hore, M. J. A.; Ford, J.; Ohno, K.; Composto, R. J.; Hammouda, B. Direct Measurements of Polymer Brush Conformation Using Small-Angle Neutron Scattering (SANS) from Highly Grafted Iron Oxide Nanoparticles in Homopolymer Melts. *Macromolecules* **2013**, *46* (23), 9341–9348. https://doi.org/10.1021/ma401975a.

(10) Doane, T. L.; Chuang, C.-H.; Hill, R. J.; Burda, C. Nanoparticle ζ -Potentials. *Acc. Chem. Res.* **2012**, *45* (3), 317–326. https://doi.org/10.1021/ar200113c.

(11) Wang, W.; Wei, Q.-Q.; Wang, J.; Wang, B.-C.; Zhang, S.; Yuan, Z. Role of Thiol-Containing Polyethylene Glycol (Thiol-PEG) in the Modification Process of Gold Nanoparticles (AuNPs): Stabilizer or Coagulant? *J. Colloid Interface Sci.* **2013**, *404*, 223–229. https://doi.org/10.1016/j.jcis.2013.04.020.

(12) Selli, D.; Motta, S.; Di Valentin, C. Impact of Surface Curvature, Grafting Density and Solvent Type on the PEGylation of Titanium Dioxide Nanoparticles. *J. Colloid Interface Sci.* **2019**, *555*, 519–531. https://doi.org/10.1016/j.jcis.2019.07.106.

(13) Rahme, K.; Chen, L.; Hobbs, R. G.; Morris, M. A.; O'Driscoll, C.; Holmes, J. D. PEGylated Gold Nanoparticles: Polymer Quantification as a Function of PEG Lengths and Nanoparticle Dimensions. *RSC Adv.* **2013**, *3* (17), 6085–6094. https://doi.org/10.1039/c3ra22739a.

(14) Selli, D.; Tawfilas, M.; Mauri, M.; Simonutti, R.; Di Valentin, C. Optimizing PEGylation of TiO2 Nanocrystals through a Combined Experimental and Computational Study. *Chem. Mater.* **2019**, *31* (18), 7531–7546. https://doi.org/10.1021/acs.chemmater.9b02329.

(15) Torelli, M. D.; Putans, R. A.; Tan, Y.; Lohse, S. E.; Murphy, C. J.; Hamers, R. J. Quantitative Determination of Ligand Densities on Nanomaterials by X-Ray Photoelectron Spectroscopy. *ACS Appl. Mater. Interfaces* **2015**, *7* (3), 1720–1725. https://doi.org/10.1021/am507300x.

(16) Rahme, K.; Chen, L.; Hobbs, R. G.; Morris, M. A.; O'Driscoll, C.; Holmes, J. D. PEGylated Gold Nanoparticles: Polymer Quantification as a Function of PEG Lengths and

Nanoparticle Dimensions. *RSC Adv.* **2013**, *3* (17), 6085–6094. https://doi.org/10.1039/C3RA22739A.

(17) Zhou, H.; Fan, Z.; Li, P. Y.; Deng, J.; Arhontoulis, D. C.; Li, C. Y.; Bowne, W. B.; Cheng, H. Dense and Dynamic Polyethylene Glycol Shells Cloak Nanoparticles from Uptake by Liver Endothelial Cells for Long Blood Circulation. *ACS Nano* **2018**, *12* (10), 10130–10141. https://doi.org/10.1021/acsnano.8b04947.

(18) Wu, J.; Chen, S. Investigation of the Hydration of Nonfouling Material Poly(Ethylene Glycol) by Low-Field Nuclear Magnetic Resonance. *Langmuir* **2012**, *28* (4), 2137–2144. https://doi.org/10.1021/la203827h.

(19) Oelmeier, S. A.; Dismer, F.; Hubbuch, J. Molecular Dynamics Simulations on Aqueous Two-Phase Systems - Single PEG-Molecules in Solution. *BMC Biophys.* **2012**, *5* (1), 14. https://doi.org/10.1186/2046-1682-5-14.

(20) Dahal, U.; Wang, Z.; Dormidontova, E. E. Hydration of Spherical PEO-Grafted Gold Nanoparticles: Curvature and Grafting Density Effect. *Macromolecules* **2018**, *51* (15), 5950–5961. https://doi.org/10.1021/acs.macromol.8b01114.

(21) Dahal, U. R.; Wang, Z.; Dormidontova, E. E. Hydration and Mobility of Poly(Ethylene Oxide) Brushes. *Macromolecules* **2017**, *50* (17), 6722–6732. https://doi.org/10.1021/acs.macromol.7b01369.

(22) de Gennes, P. G. Conformations of Polymers Attached to an Interface. *Macromolecules* **1980**, *13* (5), 1069–1075. https://doi.org/10.1021/ma60077a009.

(23) Jin, R.; Zeng, C.; Zhou, M.; Chen, Y. Atomically Precise Colloidal Metal Nanoclusters

and Nanoparticles: Fundamentals and Opportunities. *Chem. Rev.* **2016**, *116* (18), 10346–10413. https://doi.org/10.1021/acs.chemrev.5b00703.

(24) Jin, J.; Jiang, W.; Yin, J.; Ji, X.; Stagnaro, P. Plasma Proteins Adsorption Mechanism on Polyethylene-Grafted Poly(Ethylene Glycol) Surface by Quartz Crystal Microbalance with Dissipation. *Langmuir* **2013**, *29* (22), 6624–6633. https://doi.org/10.1021/la4017239.

(25) Ji, J.; Feng, L.; Qiu, Y.; Yu, X. Stearyl Poly(Ethylene Oxide) Grafted Surfaces for Preferential Adsorption of Albumin Part 2. The Effect of Molecular Mobility on Protein Adsorption. *Polymer (Guildf).* **2000**, *41* (10), 3713–3718. https://doi.org/10.1016/S0032-3861(99)00556-X.

(26) Zhang, J.; Huang, Z.; Liu, D. Efficient Protein-Repelling Thin Films Regulated by Chain Mobility of Low-T g Polymers with Increased Stability via Crosslinking. *Appl. Surf. Sci.* **2017**, *426*, 796–803. https://doi.org/10.1016/j.apsusc.2017.07.250.

(27) Maccarini, M.; Briganti, G.; Rucareanu, S.; Lui, X.; Sinibaldi, R.; Sztucki, M.; Lennox, R. B. Characterization of Poly (Ethylene Oxide) -Capped Gold Nanoparticles in Water by Means of Transmission Electron Microscopy , Thermogravimetric Analysis , Mass Density , and Small Angle Scattering. *J. Phys. Chem. C* **2010**, *114* (15), 6937–6943. https://doi.org/10.1021/jp9118088.

(28) Grünewald, T. A.; Lassenberger, A.; van Oostrum, P. D. J.; Rennhofer, H.; Zirbs, R.; Capone, B.; Vonderhaid, I.; Amenitsch, H.; Lichtenegger, H. C.; Reimhult, E. Core–Shell Structure of Monodisperse Poly(Ethylene Glycol)-Grafted Iron Oxide Nanoparticles Studied by Small-Angle X-Ray Scattering. *Chem. Mater.* **2015**, *27* (13), 4763–4771. https://doi.org/10.1021/acs.chemmater.5b01488.

(29) Marrink, S. J.; Risselada, H. J.; Yefimov, S.; Tieleman, D. P.; de Vries, A. H. The MARTINI Force Field: Coarse Grained Model for Biomolecular Simulations. *J. Phys. Chem. B* **2007**, *111* (27), 7812–7824. https://doi.org/10.1021/jp071097f.

(30) Rossi, G.; Fuchs, P. F. J.; Barnoud, J.; Monticelli, L. A Coarse-Grained MARTINI Model of Polyethylene Glycol and of Polyoxyethylene Alkyl Ether Surfactants. *J. Phys. Chem. B* **2012**, *116* (49), 14353–14362. https://doi.org/10.1021/jp3095165.

(31) Wassenaar, T. A.; Pluhackova, K.; Böckmann, R. A.; Marrink, S. J.; Tieleman, D. P. Going Backward: A Flexible Geometric Approach to Reverse Transformation from Coarse Grained to Atomistic Models. *J. Chem. Theory Comput.* **2014**, *10* (2), 676–690. https://doi.org/10.1021/ct400617g.

(32) Tay, K. A.; Bresme, F. Wetting Properties of Passivated Metal Nanocrystals at Liquid−Vapor Interfaces: A Computer Simulation Study. *J. Am. Chem. Soc.* **2006**, *128* (43), 14166–14175. https://doi.org/10.1021/ja061901w.

(33) Jorgensen, W. L.; Maxwell, D. S.; Tirado-Rives, J. Development and Testing of the OLPS All-Atom Force Field on Conformational Energetics and Properties of Organic Liquids. *J. Am. Chem. Soc.* **1996**, *118* (15), 11225–11236. https://doi.org/10.1021/ja9621760.

(34) Dahal, U. R.; Dormidontova, E. E. Spontaneous Insertion, Helix Formation, and Hydration of Polyethylene Oxide in Carbon Nanotubes. *Phys. Rev. Lett.* **2016**, *117* (2), 027801. https://doi.org/10.1103/PhysRevLett.117.027801.

(35) Dahal, U. R.; Dormidontova, E. E. The Dynamics of Solvation Dictates the Conformation of Polyethylene Oxide in Aqueous, Isobutyric Acid and Binary Solutions. *Phys. Chem. Chem. Phys.* **2017**, *19* (15), 9823–9832. https://doi.org/10.1039/C7CP00526A.

(36) Humphrey, W.; Dalke, A.; Schulten, K. VMD: Visual Molecular Dynamics. *J. Mol. Graph.* **1996**, *14* (1), 33–38. https://doi.org/10.1016/0263-7855(96)00018-5.

(37) Devanand, K.; Selser, J. C. Polyethylene Oxide Does Not Necessarily Aggregate in Water. *Nature* **1990**, *343* (6260), 739–741. https://doi.org/10.1038/343739a0.

(38) Binder, K.; Milchev, A. Polymer Brushes on Flat and Curved Surfaces: How Computer Simulations Can Help to Test Theories and to Interpret Experiments. *J. Polym. Sci. Part B Polym. Phys.* **2012**, *50* (22), 1515–1555. https://doi.org/10.1002/polb.23168.

(39) Chen, Y.; Xu, Q.; Jin, Y.; Qian, X.; Liu, L.; Liu, J.; Ganesan, V. Design of End-to-End Assembly of Side-Grafted Nanorods in a Homopolymer Matrix. *Macromolecules* **2018**, *51* (11), 4143–4157. https://doi.org/10.1021/acs.macromol.8b00292.

(40) Morgese, G.; Shirmardi Shaghasemi, B.; Causin, V.; Zenobi-Wong, M.; Ramakrishna, S. N.; Reimhult, E.; Benetti, E. M. Next-Generation Polymer Shells for Inorganic Nanoparticles Are Highly Compact, Ultra-Dense, and Long-Lasting Cyclic Brushes. *Angew. Chemie - Int. Ed.* **2017**, *56* (16), 4507–4511. https://doi.org/10.1002/anie.201700196.

(41) Dukes, D.; Li, Y.; Lewis, S.; Benicewicz, B.; Schadler, L.; Kumar, S. K. Conformational Transitions of Spherical Polymer Brushes: Synthesis, Characterization, and Theory. *Macromolecules* **2010**, *43* (3), 1564–1570. https://doi.org/10.1021/ma901228t.

(42) Savin, D. A.; Pyun, J.; Patterson, G. D.; Kowalewski, T.; Matyjaszewski, K. Synthesis and Characterization of Silica-Graft-Polystyrene Hybrid Nanoparticles: Effect of Constraint on the Glass-Transition Temperature of Spherical Polymer Brushes. *J. Polym. Sci. Part B Polym. Phys.* **2002**, *40* (23), 2667–2676. https://doi.org/10.1002/polb.10329.

(43) Cicero, G.; Calzolari, A.; Corni, S.; Catellani, A. Anomalous Wetting Layer at the Au(111) Surface. *J. Phys. Chem. Lett.* **2011**, *2* (20), 2582–2586. https://doi.org/10.1021/jz200989n.

(44) Dimitrov, D. I.; Milchev, A.; Binder, K. Polymer Brushes in Cylindrical Pores: Simulation versus Scaling Theory. *J. Chem. Phys.* **2006**, *125* (3), 034905. https://doi.org/10.1063/1.2211615.

(45) Daoud, M.; Cotton, J. P. Star Shaped Polymers : A Model for the Conformation and Its Concentration Dependence. *J. Phys.* **1982**, *43* (3), 531–538. https://doi.org/10.1051/jphys:01982004303053100.

(46) Zhulina, E. B.; Birshtein, T. M.; Borisov, O. V. Curved Polymer and Polyelectrolyte Brushes beyond the Daoud-Cotton Model. *Eur. Phys. J. E* **2006**, *20* (3), 243–256. https://doi.org/10.1140/epje/i2006-10013-5.

(47) Wijmans, C. M.; Zhulina, E. B. Polymer Brushes at Curved Surfaces. *Macromolecules* **1993**, *26* (26), 7214–7224. https://doi.org/10.1021/ma00078a016.

(48) Dan, N.; Tirrell, M. Polymers Tethered to Curves Interfaces: A Self-Consistent-Field Analysis. *Macromolecules* **1992**, *25* (11), 2890–2895. https://doi.org/10.1021/ma00037a016.

(49) Milner, S. T.; Witten, T. A.; Cates, M. E. Theory of the Grafted Polymer Brush. *Macromolecules* **1988**, *21* (8), 2610–2619. https://doi.org/10.1021/ma00186a051.

(50) Murat, M.; Grest, G. S. Structure of a Grafted Polymer Brush: A Molecular Dynamics Simulation. *Macromolecules* **1989**, *22* (3), 4054–4059.

https://doi.org/10.1021/ma00200a041.

(51) Ohno, K.; Morinaga, T.; Takeno, S.; Tsujii, Y.; Fukuda, T. Suspensions of Silica Particles Grafted with Concentrated Polymer Brush: Effects of Graft Chain Length on Brush Layer Thickness and Colloidal Crystallization. *Macromolecules* **2007**, *40* (25), 9143–9150. https://doi.org/10.1021/ma071770z.

(52) Gombotz, W. R.; Guanghui, W.; Horbett, T. A.; Hoffman, A. S. Protein Adsorption to Poly(Ethylene Oxide) Surfaces. *J. Biomed. Mater. Res.* **1991**, *25* (12), 1547–1562. https://doi.org/10.1002/jbm.820251211.

(53) Schöttler, S.; Becker, G.; Winzen, S.; Steinbach, T.; Mohr, K.; Landfester, K.; Mailänder, V.; Wurm, F. R. Protein Adsorption Is Required for Stealth Effect of Poly(Ethylene Glycol)- and Poly(Phosphoester)-Coated Nanocarriers. *Nat. Nanotechnol.* **2016**, *11* (4), 372–377. https://doi.org/10.1038/nnano.2015.330.